

Design, Analysis and Simulation of Magnetic Biased Inductors with Saturation-Gap

Aguilar, Andres Revilla; Munk-Nielsen, Stig

Published in:

Proceedings of the 16th Conference on Power Electronics and Applications, EPE'14-ECCE Europe

DOI (link to publication from Publisher):

[10.1109/EPE.2014.6910896](https://doi.org/10.1109/EPE.2014.6910896)

Publication date:

2014

Document Version

Early version, also known as pre-print

[Link to publication from Aalborg University](#)

Citation for published version (APA):

Aguilar, A. R., & Munk-Nielsen, S. (2014). Design, Analysis and Simulation of Magnetic Biased Inductors with Saturation-Gap. In Proceedings of the 16th Conference on Power Electronics and Applications, EPE'14-ECCE Europe IEEE Press. <https://doi.org/10.1109/EPE.2014.6910896>

General rights

Copyright and moral rights for the publications made accessible in the public portal are retained by the authors and/or other copyright owners and it is a condition of accessing publications that users recognise and abide by the legal requirements associated with these rights.

- Users may download and print one copy of any publication from the public portal for the purpose of private study or research.
- You may not further distribute the material or use it for any profit-making activity or commercial gain
- You may freely distribute the URL identifying the publication in the public portal -

Take down policy

If you believe that this document breaches copyright please contact us at vbn@aub.aau.dk providing details, and we will remove access to the work immediately and investigate your claim.

Design, Analysis and Simulation of Magnetic Biased Inductors with Saturation-Gap

Andres Revilla Aguilar & Stig Munk-Nielsen
Aalborg University
Pontoppidanstraede 101. 9220-DK
Aalborg East, Denmark
Tel.: + 45 9940 9240
E-Mail: are@et.aau.dk; smn@et.aau.dk
URL: <http://www.et.aau.dk>

Keywords

«Device simulation», «Magnetic device», «Passive component», «Emerging topology».

Abstract

Permanent magnet biasing, is a known technique for increasing the energy storage capability of inductors operating in DC applications. The opposing flux introduced by a permanent magnet will extend the saturation flux limit of a given magnetic material. When full biasing of the core is achieved, the effective saturation current limit of a given inductor is doubled. This results in a smaller requirement in number of turns and area cross-section, allowing for smaller and/or more efficient inductors. By adding some switching elements, the benefits of biased inductors can also be used in AC applications. This paper presents a review of the scientific literature on biased hybrid inductors and the evolution of the used magnets and cores configurations. A recently developed biasing configuration, *the saturation-gap*, will also be analyzed and the design parameter will be identified using finite element software. The simulation results will be compared with empirical laboratory measurements on physical units.

1. Introduction

The use of permanent magnets for bias magnetization is a known technique for increasing the energy storage capability of DC inductors, resulting in a size reduction or increased efficiency. Full biasing allows for a reduction of 50% in either core cross-sectional area or number of turns [ref]. This will result in a 50% smaller core or 50% lower copper losses, respectively. A compromised distribution of the reduction factor is desired in most cases. The total inductor size and losses reduction will be dependent of the specific inductor design and application. Even if the first studies of the subject date back to the early 1960's, only a limited amount of scientific papers has been published since. The focus of the available publications covers different topics: The analysis of benefits using permanent magnet biasing, development of techniques for optimal inductor design, and practical test on physical inductors with different configurations of permanent magnets and soft magnetic core shapes. Fig. 1. shows the timeline of publications. The public research on this technique has been absent for almost four decades. In the last decade a small amount of papers has been published. During this time, the advancements on the subject have been almost limited to patent publications. More than 20 patents have been found on the subject. In [11] we presented a new biasing configuration, *the Saturation-gap*. This configuration is proven to achieve full biasing in ferrite and iron materials [11][12]. It uses standard non-gapped core shapes and it is free from patent restrictions.

The following section 2 presents a brief theoretical background on permanent magnets and inductor biasing and design. Section 3 summarizes the state of the art with the evolution of the different design approaches found in the literature. In section 4 a finite element analysis of *the Saturation-gap* topology

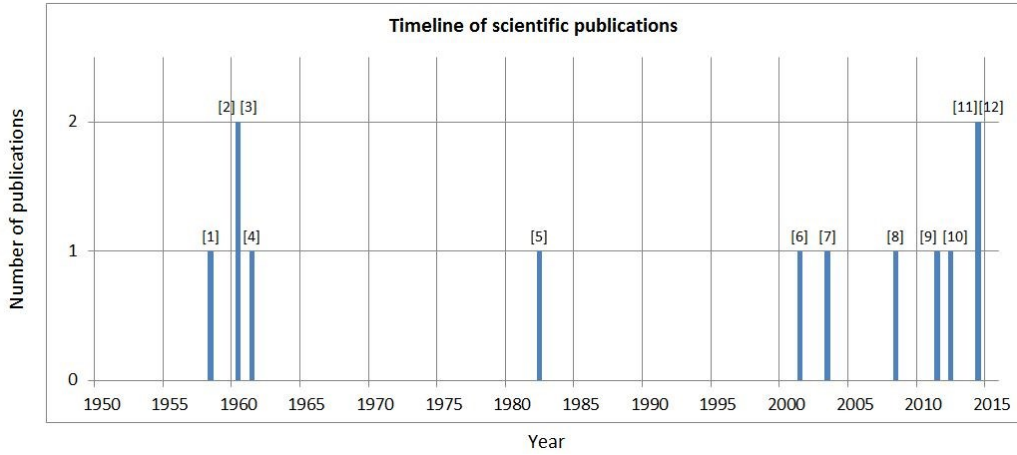


Fig. 1. Timeline of scientific publications on magnetic biased inductors. Numbers in square brackets are the references number.

will be used in order to characterize its operation and identify the relevant parameters for this hybrid inductor design. Finally section 5 presents the conclusions and future research on the subject.

2. Background theory

Inductors intended for DC applications present a highly asymmetric magnetizing current. Their working point on the load line is restricted to the first quadrant. The energy storage capability on the third quadrant is totally unused. Hybrid inductors, uses permanent magnets in order to introduce a negative bias flux in the core material and accordingly extend its maximum DC flux limit.

In Fig. 2. it is sketched the BH loop of a hypothetical inductor, we will concentrate in its linear region. In the case of a standard DC inductor (Fig. 2.a) the maximum allowable flux density will be that of saturation, B_{sat} . When introducing an opposing magnetic bias, $-B_{bias}$, the maximum flux excursion will be the sum of B_{sat} plus B_{bias} (Fig. 2.b). The maximum allowable biasing flux will be equal to the saturation flux of the core. It can be graphically appreciated that when full biasing is achieved the energy capacity (green areas) has increased by a factor of four and the core energy loss per cycle (red areas) has only increased by a factor of two. We can define that full biasing is achieved when the

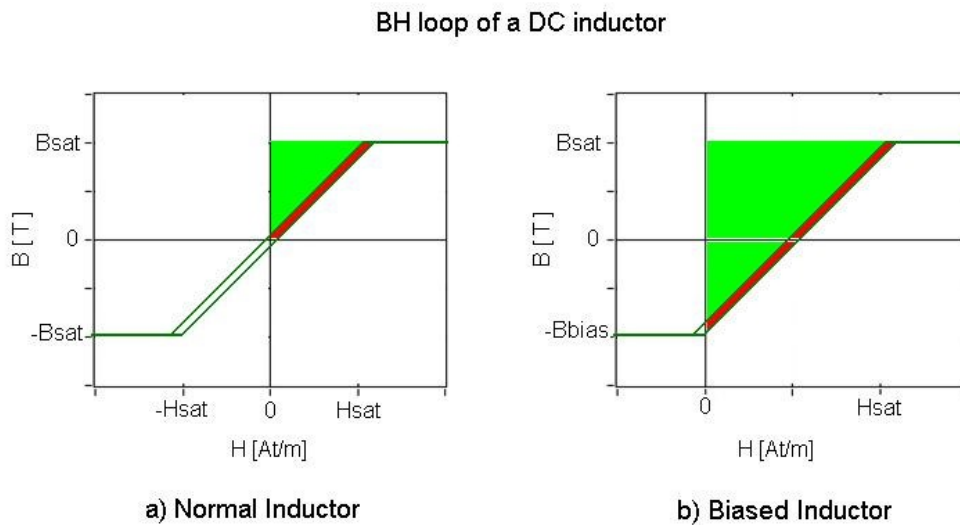


Fig. 2. Linear BH loop of normal and biased inductors. Green areas represent energy stored. Red areas represent energy loss per cycle.

BH curve of a linear PM

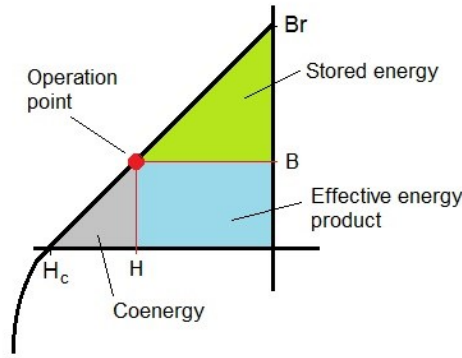


Fig. 3. BH curve of a linear PM. Green area represents energy stored in the permanent magnet. Blue area is the effective energy or BH product. Operation point is defined by the external H field. The grey area is representative of the magnetic coenergy.

initial operation point (at zero current) of the core is at the edge of the saturation knee in the third quadrant. That would be full linear biasing. If applying more biasing flux, the energy capacity will be greatly increased and the inductor will present non-linear inductance profiles characterized by very low inductance at zero current and a positive slope inductance versus current profile [11].

Typical core materials are used for their properties as magnetic conductors, presenting high permeability. On the other hand, their magnetic energy capacity is very low for practical applications. An air-gap cut into the core is typically used for energy storage. Distributed air-gap materials are another possibility. In hybrid inductor design is important to mention that the biasing flux is only required in the core material, since the saturation flux density of the core is the limiting factor.

In order to introduce the biasing flux, a permanent magnet is used. Fig. 3. presents a generic load line of a linear magnet and the areas representing energy storage and effective energy product. Ferrite, NdFeB and SmCo magnets are known to presents a linear load line in the second quadrant. If the operation point of a PM is brought below the knee of its linear region, demagnetization effects will take place. The operation point of the PM can be calculated as a function of the applied demagnetizing field, H . In cases where no demagnetization field is applied, the operation point is dependent on the ratio between the PM internal reluctance, R_{PM} and the load reluctance, R_l . [13]-[15] The actual flux value, ϕ at operation point of the magnet is calculated by:

$$\phi = A_{cPM} B = A_{cPM} (B_r + \mu_{PM} H) = \frac{H_c l_{PM}}{R_{PM} + R_l} \quad (1)$$

Where B_r , is the remanent flux density, H_c is the coercive force of the used material, μ_{PM} is the permeability of the PM material and l_{PM} is the PM length through its axes of magnetization. The PM internal reluctance is defined by:

$$R_{PM} = \frac{l_{PM}}{\mu_{PM} A_{cPM}} \quad (2)$$

The load reluctance, R_l will be defined by the materials surrounding the magnetic poles. In hybrid inductor configurations, this reluctance is defined by the core material. The permeability of the core is a non-linear function of the instantaneous flux density. Accordingly, the load reluctance, R_l is a function of the applied current in the inductor windings.

Laminated steel materials present high saturation flux density, at expenses of a high electric conductivity. They are typically used in low frequency applications. On the other hand ferrite type

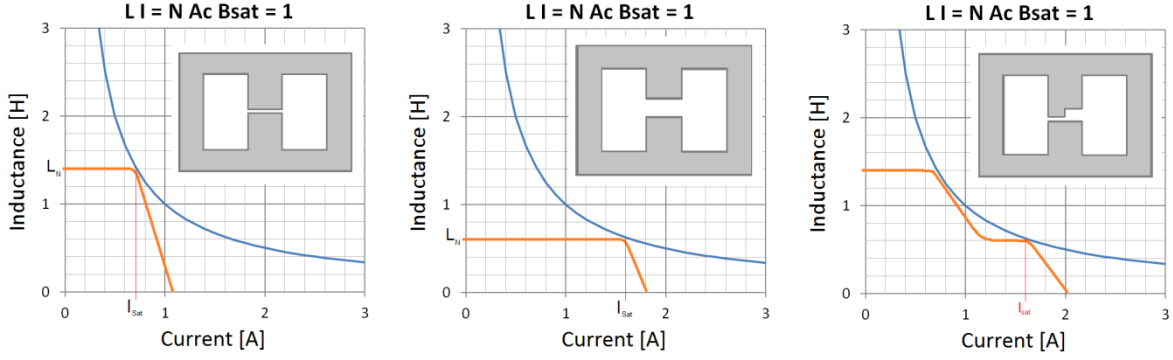


Fig. 4. LvsI profile of an inductor as function of air-gap length. Blue curve is a generic unity LI product region. Orange line represents the LvsI profile for each air-gap length. Left: short air-gap; Center: long air-gap; Right: non-constant length air-gap.

materials offer lower electric conductivity at expenses of a lower saturation flux density. These are typically used in high frequency applications, where eddy currents will be a dominant factor. PM materials can offer similar compromises. Ferrite magnets will produce the lower flux level while having the lower electric conductivity. Sintered NdFeB magnets will present the highest flux levels at expenses of a high electric conductivity. A compromise PM material can be done by using a NdFeB material bonded with resin. SmCo magnets preset lower flux levels than NdFeB, but present better thermal stability.

The relationship between the inductance, L and current, I requirements and the physical inductor design parameters is given by:

$$LI = B_{sat}NA_c \quad (3)$$

Were B_{sat} is the saturation flux density of the core material, A_c is the area cross-section of the core and N is the number of turns. Full biasing will double the flux limit, and the required NA_c product can be reduced by a factor of two. The LI product is a constant of each specific design, and it defines the maximum operation area into the LvsI profile of a given inductor design. In order to define a nominal inductance range, the air-gap length must be adjusted. Assuming the total reluctance is dominated by the air-gap we can define the nominal inductance by:

$$L = \frac{N^2}{R_g} = \frac{\mu_0 A_c N^2}{l_g} \quad (4)$$

Where R_g is the reluctance of the air-gap, μ_0 is the permeability of air and l_g is the length of the air-gap. Fig. 4. presents a unity LI product region and the LvsI profile of three hypothetical air-gaps. The use of non-constant length air-gaps will produce non-linear LvsI profiles and can optimize the used LI product.

By adding some switching elements, a biased DC inductor can be used in AC applications. In order to verify this possibility a small simulation was made using LTspice. Fig. 5. shows the schematic and the simulation results. The same sinusoidal stimulus was use in two different inductors: a standard AC inductor, and a hybrid DC inductor with a four thyristors switch. It can be appreciated how the line currents (IRgrid) in both cases are identical while the current in the DC inductor is always positive. The simulation results indicate that the use of a thyristor switching arrangement can extend the usability to AC applications while having the benefit from the size reduction advantages of a hybrid biased inductor.

PM biased inductor switching for AC applications

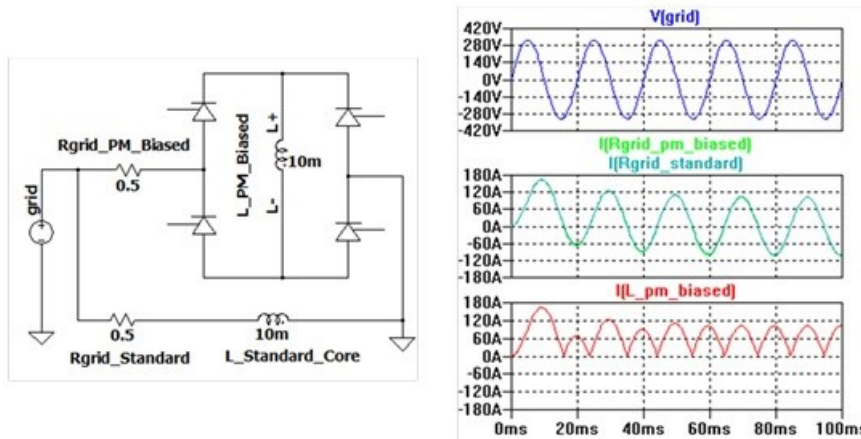


Fig. 5. Simulation of permanent magnet biased DC inductor performing on AC by the use of thyristor switching arrangement. Top curve is voltage AC stimuli; Middle curves are current through series resistors, both curves are identical; Bottom curve is current at the PM biased inductor.

3. State of the art

The specific core and magnet configurations used in hybrid inductors have been evolving from its early stages. The basic characteristics and the advantages and limitations of the different configurations found in the literature will be indicated.

Basic configuration: Magnet inside the air-gap.

The first designs of magnetic biased inductors consisted of standard gaped inductors with a permanent magnet inserted in the air-gap [1]-[4][6]-[8]. Fig. 6. shows the basic configuration. Red vectors represent flux produced by the coil and green vectors represents flux produced by the PM. This arrangement can effectively produce a certain amount of bias flux. There is however several limitations intrinsic to this configuration:

- The flux from the coil is passing directly through the magnet. Demagnetization and eddy currents become a design limitation when selecting a permanent magnet material.
- The area cross section of the magnet cannot be bigger than the cross section of the core. This implies a limitation in the maximum producible bias flux.

Hybrid configuration: Magnet Inside Air-Gap

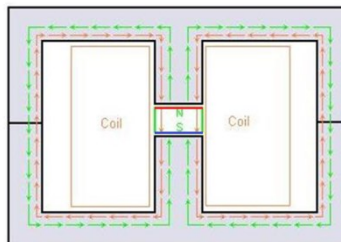


Fig. 6. Basic configuration. Permanent magnet inside air-gap. Red vector represent flux from the coil. Green vectors represent flux from the PM.

Hybrid configuration: Magnets Outside Air-Gaps

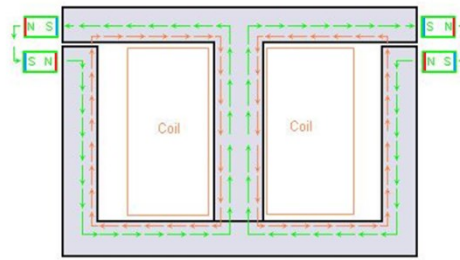


Fig. 7. Magnets in the vicinity of air-gaps. Red vector represent flux from the coil. Green vectors represent flux from the PM.

Magnets in the vicinity of the air-gaps

In order to overcome the limitations of placing the PM inside the air-gap, a logical approach has been to place the PMs in the vicinity of the air-gaps. This configuration requires special core shapes and the relevant documentation is mostly limited to patent documents. Only three scientific publications [5][8][9] have been found regarding the design of this hybrid configuration. Fig. 7. presents an inductor configuration having the biasing magnets in the vicinity of the air gaps.

Having the magnets outside the core and out of the path of the coil's flux present several advantages. The size of the magnets, and accordingly the amount of bias flux, it is no longer limited by the area cross section of the core. The flux-path of the coil is not crossing the PM. Accordingly, variations in the coil's flux will not induce EMF in the PM material and eddy currents will not be directly produced. On the other hand, a smaller level of indirectly induced eddy currents will be present in the magnet. Indirect eddy currents are stimulated by variations in the PM operation point, rather than variations in the coil's flux acting on the PM material. From (1) can be calculated the amount of PM flux variations as function of the variations of R_l . Eddy currents produce through reluctance variations will be lower than through direct induction and high flux density and low resistivity magnets like sintered NdFeB can be used in these configurations. This allows for higher bias flux levels than with the basic magnet inside the gap configurations. These benefits come at expenses of using nonstandard core shapes which require an individual design and manufacturing process. The use of nonstandard core shapes also difficult the design and optimization of the inductor.

Combination of ferrite and distributed air-gap materials

Another alternative to core with air-gaps is the use of distributed air-gap materials (DGM) or a combination of. Recently, a private company published some details about a new biased inductor

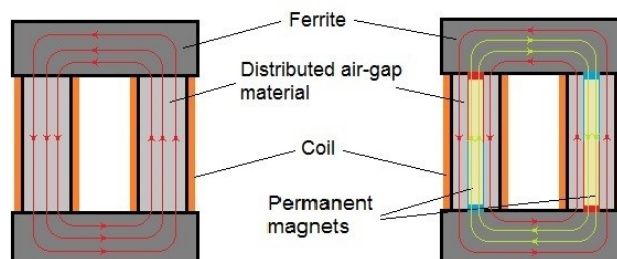


Fig. 8. Inductor configuration using a combination of ferrite and distributed air-gap material. Left: standard; Right: possible hybrid configuration. Red vectors represent flux from the coils. Green vectors represent flux from the PMs.

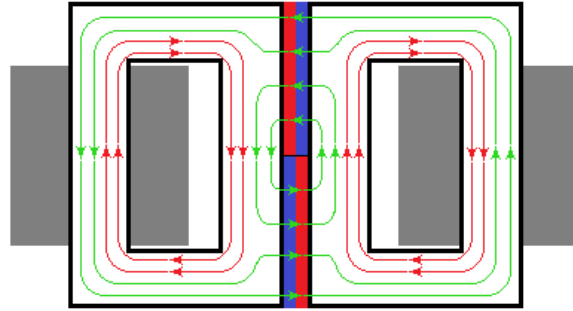


Fig. 9. The Saturation-gap biasing configuration. Red vectors represent flux from the coils. Green vectors represent flux from the PMs.

design [16]. The publication does not disclose the actual placing of the magnets, but the used topology can be accomplished with a combination of ferrite and DGM. Fig. 8. shows a configuration with a combination of materials and its possible hybrid version. This configuration uses two single layer coils wound on cylindrical segments of a DGM. The two cylinders with coils are connected using ferrite segments with square section. This topology is normally used in high frequency and high power applications, since it presents a better thermal performance compared to standard gapped cores [17][18]. A possible strategy could be to introduce the PMs inside the distributed air-gap material. Since the saturation flux density of DGM is quite high, the required A_c it is defined by the ferrite sections and the A_c of the DGM cylinders can easily allow space for the PMs. The permeability of the ferrite sections it is typically 50 to 500 higher than distributed air-gap materials. Accordingly, the flux from the PMs will be mostly concentrated through the ferrite sections, producing the desired bias.

Magnets on un-gapped cores: The Saturation-Gap

In [11][12] we developed and presented a new biasing configuration where some of the limitations mentioned for the previously configurations are addressed. This new core-magnet configuration consists of externally placed permanent magnets and standardized magnetic cores with no air gaps. The function of the permanent magnets in this configuration is a twofold: to produce saturation in a localized segment of the core which will behave as a virtual air gap (the saturation-gap section) and to create a biasing flux in the rest of the core. Fig. 9. shows the *Saturation-gap* configuration. Red vectors represent flux from the coils, green vectors represent flux from the PMs. Flux lines in The *saturation-gap* concept was tested in two different inductor applications: in [11] an EE30 ferrite core operating as a flyback transformer is been used and its saturation current extended more than double; in [12] a hybrid inductor design using iron laminations is presented. Fig. 10. shows the half size core reduction strategy which was also implemented in physical units. This strategy uses the total reduction factor to the required A_c in order to achieve minimal core weight. The number of turns in each winding is equal to the number of turns in the standard design. The A_c of the UI cores is $\frac{1}{4}$ of the standard design. The total perimeter of the hybrids A_c (including the two UI coils) will be equal to the perimeter of the A_c of the standard design. Single layer coil inductors will present the same copper resistance. Additional coil layers will introduce an increment in the hybrid coils resistance up to a

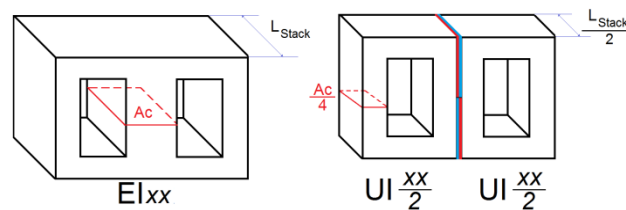


Fig. 10. Half core size reduction, design strategy with saturation-gap. A standard EI core is replaced by two UI cores with half the stack length.

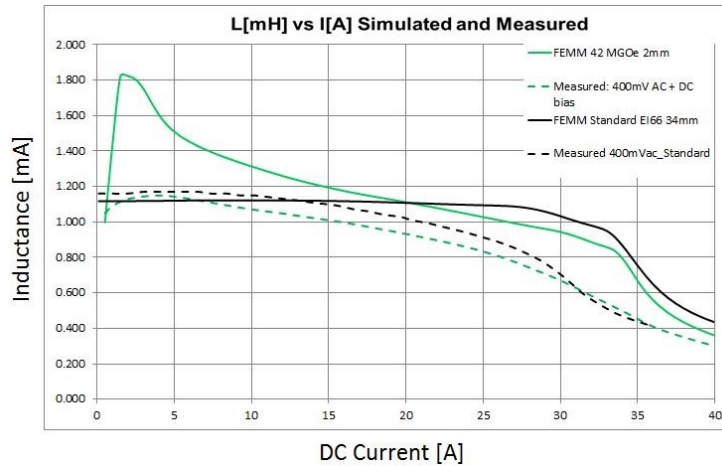


Fig. 11. Standard and Hybrid inductors measured and simulated Inductance versus DC current. Measured with WK3260B magnetic analyzer: Stimuli is 400mV AC 300Hz for a set of DC bias currents. Simulated with FEMM.

30%. This increase in the copper resistance of the hybrid inductor is also avoided when using the hybrid design to replace two individual inductors sharing the same DC current.

In [12] the basic hybrid inductor design strategy and a simulation analysis using magnetic equivalent circuit (MEC) modeling was presented. Empirical measurements on physically units were also performed. The experimental results showed a 50% smaller core in the hybrid configuration, while presenting a slightly lower inductance. The measured LvsI profile of the two units can be seen in the dashed lines in Fig. 11. The MEC simulation results were not accurate enough for design purposes. On the other hand, they provided a good analysis of the different operation behaviors found in the saturation-gap configuration. MEC simulations uses very approximated models of the overall geometry. In the following section, a finite element analysis of the physical units presented in [12] is performed using FEMM. This analysis will be used to characterize more precisely the behavior of this configuration and to identify the specific PM dimensions required for the design of the equivalent air-gap.

4. Finite Element Analysis

The standard and the hybrid design presented in [12] were analyzed using FEMM software. The standard design uses EI66 laminations with stack length of 34 mm. The hybrid design uses two UI30 cores with 20 mm of stack length. The used magnets are 2 mm length NdFeB 42MGOe. Each coil has

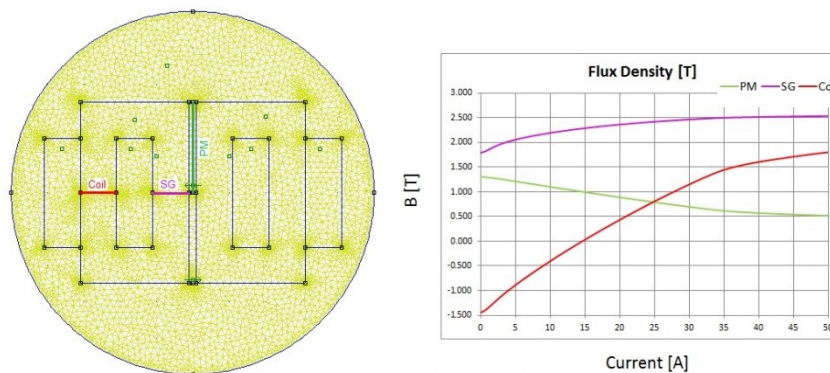


Fig. 12. Flux density as function of current. Values are measured in FEMM model as the average flux density at each position of the marked color lines. Red: flux density inside the coil (*Coil*); Purple: flux density at the saturation-gap region (*SG*) and Green: Permanent magnet flux density (*PM*).

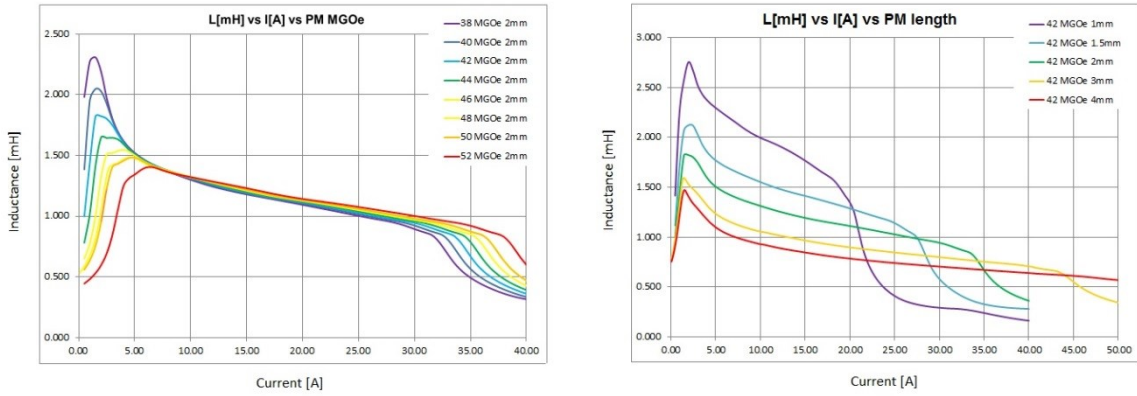


Fig. 13. Inductance versus current for different PMs. FEMM simulations. Left: Different NdFeB grades in MGOe units; Right: Different PM lengths through magnetization axes.

36 turns of 2.25 mm diameter copper wire. The an-hysteretic DC BH curve of the laminations material was used in the FEMM models. The two physical units were also tested with a WK3260B magnetic analyzer. The $LvsI$ profiles were measured using a 400mV AC stimulus over a range of DC bias currents. FEMM uses magneto-static based calculations. In order to calculate the incremental inductance, the analysis is repeated for a set of currents, ranging from zero to 50A in increments of 0.5A. Since the analysis is magneto-static, eddy currents in the core or in the permanent magnets are not considered by the simulations.

Fig. 11. shows the measured and simulated $LvsI$ profiles of the standard and the hybrid inductor designs. The measured curves present lower inductance values, especially close to the saturation current. It is known that the effective permeability of a magnetic material will present differences when using different stimuli. When DC stimuli are applied the irreversible permeability effects will be dominant. When small signal AC is applied over DC bias current levels, the reversible permeability effects are the dominant factor. The measured inductance using small AC stimuli will present lower inductance values, since the slope of the small BH loop will always be lower than the actual incremental slope [19].

It can also be noticed quite some differences in the hybrid inductance at currents below 5A. The lower inductance values, in the measured result, are related to the effects of indirectly induced eddy currents in the PMs. These effects will be more clearly understood after looking at some of the result of the FEMM analysis. Fig. 12. shows the FEMM model of the hybrid inductor and the flux density levels as a function of current. The three curves are the average flux density at the positions marked by the color lines. These simulation results confirm the expected flux behavior in a saturation-gap configuration according to the MEC analysis presented in [12]. At zero current the flux density at *Coil* is -1.5 T, this value can be defined as the limit of the linear region of the core. Accordingly, the simulation indicates

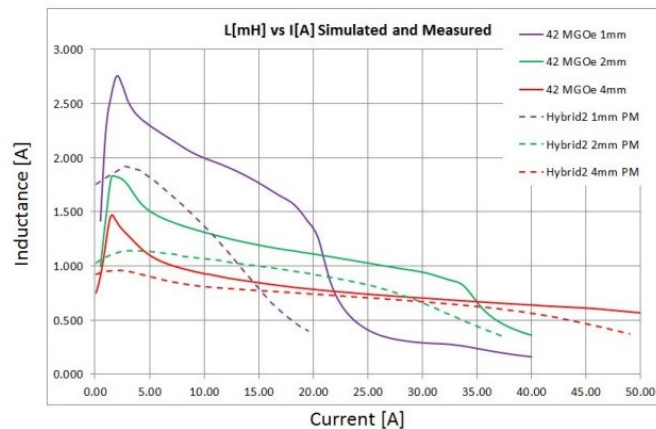


Fig. 14. Inductance versus current for three PM lengths. Calculated with FEMM (solid lines) and measured with WK3260B (dashed lines).

full bias is been achieved. The current can increase up to 35A until the flux density at *Coil* reaches the positive saturation of the core, 1.5 T. The flux density at the *SG* region starts at 1.7 T and slowly increases, approaching a Quasy-Saturated Equilibrium (QSE) below 2.5 T. The flux present at *SG* is the addition of the coil and the PM fluxes. In the DC current range, from 4A to 35A approximately, the model is working in its linear region. As the flux from the coil is increasing with current, the QSE at the *SG* is maintained by the PMs lowering its operation point. Energy is been stored in the PM. In the current range from 0A to 4A approximately, the model is working in its non-linear region. The initial flux at *SG* has not yet reached the QSE and the slope of the flux at *Coil* and at *SG* is not constant. Non-linear inductance effects can be undesired or wanted depending on the different inductor applications [18]. In order to analyze the parameters defining the range and value of the linear and non-linear inductance, additional FEMM simulation were performed. Fig. 13. shows the LvsI curves of the model for different PM lengths and strengths. In the left plot can be noticed the effect of using different PM strengths. The simulated PM are NdFeB with energy density products ranging from 38 MGOe to 52 MGOe, which are commercially available. It can be noticed that the PM strength is defining the maximum saturation flux and the initial flux condition, controlling the possible non-linear inductance effects. On the right plot of Fig. 13. the LvsI values are presented for different PM lengths. It can be noticed a clear dependency of the PM length and the equivalent saturation air-gap. The QSE level will define the linear inductance value. For a given core material, the QSE value is only dependent on the core and magnets relative geometry while being independent of the PM strength. Comparing the measured and simulated results in Fig. 11. can be noticed differences in the non-linear inductance range. Fig. 14. shows the measured and simulated results for three PM lengths. It can be noticed a clear correlation. On the other hand, measured values tend to be lower, especially at the non-linear inductance range. The differences become greater as the PM length is decreased. This can be understood by the behavior of indirect eddy currents in the PMs. Indirect eddy currents, will tend to maintain the operation point of the PMs. In the hypothetical case of a superconducting magnet (0 Kelvin) the operation point will be always maintained by the eddy currents. In normal conditions, eddy currents will present resistive losses and the operation point will not be constant. From (1) can be seen the dependency on the PM flux variations as function of variations in load reluctance, R_l . The amplitude of the EMF inducing the eddy currents will be inversely proportional to the PM internal reluctance R_{PM} . Accordingly, magnets with smaller R_{PM} (shorter length) will present higher eddy currents and the simulated behavior will differ more from the measured valued.

5. Conclusions and further research

The Saturation-gap biasing configuration has been implemented on a laminated steel 1mH 20A DC link choke. The hybrid design uses standard UI30 laminations, and presents 50% smaller core while almost matching the LvsI profile of the standard EI66 design. The presented designs have been analyzed using FEMM. The simulation results present higher inductance values compare to the empirical measurements. FEMM analysis is magneto-static and therefore does not account for eddy current effects. Indirectly induced eddy currents in the magnets will tend to maintain the operation point of the PM towards the B_r value, resulting in more flux and higher reluctance through the saturation-gap region. The FEMM analysis presents the required resolution for the design of hybrid inductors with the saturation-gap. PM length and strength have been identified as the parameters controlling the equivalent air-gap dimensions defining the linear and/or non-linear LvsI profile. The flux analysis with FEMM is consistent with the behavior observed with MEC simulations in [12]. The QSE value will define the nominal inductance and it will be dependent on the saturation knee profile of the core material and the PM length, while being independent from the PM strength. NdFeB magnets with 42 MGOe maximum energy density products were used to produce a linear LvsI profile. PMs with lower MGOe values will tend towards non-linear inductance profile with negative slopes. PMs of higher strength will tend towards non-linear inductance with positive slope. Further research will focus on the simulation of the eddy current effects and their role in the LvsI shape. The core losses measurements presented in [11][12] shows an unexpected profile, having higher losses at lower currents and lower losses at higher currents. A deeper investigation of the involved loss mechanisms will be also a focus for further research.

References

- [1] J.T. Ludwig, "Design of optimum inductors using magnetically hard ferrites in combination with magnetically soft materials," *Journal of Applied Physics*. Volume 29, Issue 3, pp. 497-499. Mar 1958.
- [2] J.T. Ludwig, "Inductors biased with permanent magnets. Part I: Theory and analysis," *American Institute of Electrical Engineers, Part I: Communication and Electronics, Transactions of the*. Volume 79, Issue 3, pp. 273-278. July 1960.
- [3] J.T. Ludwig, "Inductors biased with permanent magnets. Part II: Design and synthesis," *American Institute of Electrical Engineers, Part I: Communication and Electronics, Transactions of the*. Volume 79, Issue 3, pp. 278-291. July 1960.
- [4] J.T. Ludwig, "Inductors biased with permanent magnets," *Electrical Engineering*, Volume 80, Issue 6, p 408. June 1961.
- [5] Akio Nakamura, and Junpei Ohta, "A new reverse-biased choke coil," *Proceedings of Powercon 9 C-5*. TDK-Electronics Company Ltd. Power Concepts, Inc. July 1982.
- [6] Kuo Baoquan, Song Liwei, Zhang Qianfan, and Cheng Shukang, "The principle and design of the permanent magnet bias DC reactor," *Proceedings of the Fifth International Conference on Electrical Machines and Systems, ICEMS 2001*. Volume 1, pp. 230-232. August 2001.
- [7] Teruhiko Fujiwara, and Hatsuo Matsumoto, "A new downsized large current choke coil with magnet bias method," *Telecommunications Energy Conference, 2003. INTELEC '03. The 25th International*. IEEE, pp. 416-420. October 2003.
- [8] Rafal Wrobel, Neville McNeill, and Phil H. Mellor, "Design of a high-temperature pre-biased line choke for power electronics applications," *Power Electronics Specialists Conference. PESC 2008*. IEEE, pp 3171–3177. Jun 2008.
- [9] G.M. Shane, and S.D. Sudhoff, "Permanent magnet inductor design," *Electric Ship Technologies Symposium, IEEE*, pp. 330-333. 10-13 April 2011.
- [10] G.M. Shane, and S.D. Sudhoff, "Design and Optimization of Permanent Magnet Inductors," *Applied Power Electronics Conference and Exposition (APEC) 2012, 27th Annual IEEE*, pp 1770 – 1777. Feb 2012.
- [11] Andres Revilla Aguilar, and Stig Munk-Nielsen, "Method for introducing bias magnetization in ungaped cores: The Saturation-Gap," *Applied Power Electronics Conference and Exposition (APEC) 2014, 29th Annual IEEE*, pp 721 - 725. 16-20 March 2014.
- [12] Andres Revilla Aguilar, Stig Munk-Nielsen, Marco Zuccherato and Hans-Jørgen Thougard, "Size reduction of a DC line choke using saturation gap and biasing with permanent magnets," *PCIM Europe 2014*, pp 1667 – 1674. 20-22 May 2014.
- [13] C.M. Andrews, "Understanding permanent magnets," *TECH Notes Group Arnold*.
- [14] H. Lovatt and P. Watterson, "Energy stored in permanent magnets," *IEEE Transactions on Magnetics*, 35(1) pp 505-507, Jan. 1999.
- [15] David Meeker, "Magnetic Circuit Derivation of Energy Stored in a Permanent Magnet," *FEMM online documentation*, <http://www.femm.info/wiki/PMEnergy>.
- [16] Stefan Herzog, Alexander Stadler and Christof Gulden, "MaxFlux–Magnetically Biased Inductor," *Bodo's Power*, Jun 2014.
- [17] Alexander Stadler, Tobias Stolzke and Christof Gulden, "Design and simulation of high power filter inductors with minimized thermal resistance," *PCIM Europe 2014*, pp 1652 – 1658. 20-22 May 2014.
- [18] Alexander Stadler, Christof Gulden and Tobias Stolzke, "Nonlinear inductors for active power factor correction circuits," *EPE-PEMC 2012 ECCE Europe*, pp LS7b-2.1-1 - LS7b-2.1-4. 4-6 Sept. 2012.
- [19] Jörn Schlieve, Stefan Schefler and Stefan Weber, "Simulating saturation behavior of inductive components," *PCIM Europe 2014*, pp 542 – 549. 20-22 May 2014.